

# IDENTIFICATION OF HAIRPIN-TYPE FLOW STRUCTURES IN SEPARATED FLOW BEHIND A THREE-DIMENSIONAL HILL USING POD

Sylvain Lardeau  
Fabrizio Tessicini  
Michael A. Leschziner

Imperial College London, Department of Aeronautics  
Prince Consort Road, South Kensington  
London, UK, SW7 2AZ  
Email: s.lardeau@imperial.ac.uk

## ABSTRACT

The characteristics of large-scale, periodic features associated with separation behind a three-dimensional hill-shaped obstruction in a duct are explored using proper orthogonal decomposition (POD) and extended POD, with particular emphasis being placed on the question of whether or not these features depend on the Reynolds number. Despite the wide range of Reynolds number investigated ( $Re = 1300$ ,  $Re = 13,000$  and  $Re = 130,000$ ), significant similarities among corresponding low-order POD modes and in the flow structure of the reconstructed flow fields for the three flows are found. These suggest a single mechanism for the formation of large-scale features associated with periodic shedding, regardless of the Reynolds number. The POD spectra also show strong similarities, especially above  $Re=13,000$ .

## INTRODUCTION

For over two decades, a large proportion of the research into wall-turbulence has been devoted to identifying distinct types of structure in sheared near-wall layers. It is now commonly accepted that near-wall flows are dominated, at least at relatively low Reynolds numbers, by large-scale, energetic, hairpin-like, vortical structures, with legs anchored close to the wall and heads extending to the middle part of the boundary layer (Zhou et al., 1999). These structures are continually deformed by shear into elongated streamwise streaks that are self-sustaining or self-regenerating (Jimenez and Pinelli, 1999). One important reason for the intense interest in coherent-structure identification and classification is that friction drag is closely linked to the near-wall structures, and any promising attempt to control drag rely on a modification of these structures or an intervention into the mechanism that sustain them - although there is uncertainty on whether the above structural mechanisms, observed at low values of the Reynolds number, pertain to the much higher values encountered in practice.

While hairpin-shaped vortices have been studied principally in the context of simple near-wall shear, very similar structures have been observed in other wall-bounded configurations, including ones in which near-wall layers are subjected to major distortions by geometric obstacles. One example is the flow around a hemisphere on a flat wall, studied extensively by Acarlar and Smith (1987). Based on observations of the behaviour of large-scale structures in the flow, Acarlar and Smith (1987) characterise the flow as comprising three distinct parts: the tip - located between two subsequent hairpin vortices, the head - located near the top part of the flow, and the legs - dominated by streamwise

vorticity. The head contains both transverse and streamwise vorticity, which makes its visualisation difficult using classical tools. Regular patterns are observed up to  $Re_R = 3400$  (with  $R$  being the radius of the hemisphere). At higher values, however, these coherent structures become elusive, and their existence is somewhat speculative. One important parameter in this respect is the size of the sphere compared to boundary layer thickness. For low values of this ratio, and at low Reynolds number, hairpins created by the hemisphere tend to be assimilated into the hairpins created *naturally* within the turbulent boundary layer. At higher Reynolds number, however, the size of hairpins in the boundary layer, scaled on the viscous layer, is small and then there is a scale separation between the two families of hairpin structures.

Two further examples in which hairpin vortices have been observed are, first, the flow behind a triangular tab on a flat plate, in which Dong and Meng (2004) described the existence of  $\Omega$ -shaped vortices downstream of the tab; and second, the flow behind a hemispherical pimple on a cylinder aligned in the streamwise direction, in which Hsieh and Wang (1996) found hairpin-type structures aft of the pimple.

This paper reports an investigation into the flow structure, in general, and hairpin-shaped features, in particular, in the wake following separation from the leeward side of a 3d hill-shaped obstacle immersed in a turbulent flat-plate boundary layer (within a duct) of thickness 0.5 times the hill height at a Reynolds number of 130,000 (based on the hill height and free-stream velocity). This configuration has become, over the past 5 years, a popular test case for RANS and LES prediction schemes. This popularity stems from the combination offered by this case of geometric simplicity, physical complexity - associated with a generic separation from a curved surface - and the availability of very detailed LDA and HWA experimental data reported by Simpson et al. (2002). Among a number of computational studies for this case reported over the past two years, that of Tessicini et al. (2007), undertaken with LES and hybrid LES-RANS methods, is probably the most comprehensive, and this also reviews earlier studies. All these studies focused, almost exclusively, on mean-flow properties - in particular, the flow topology on the hill surface, the mean velocity and the turbulence energy. However, the paper by Tessicini et al also contains a brief discussion of some unsteady features, including a fleeting exposure of the vortical structure in the wake behind the hill. In contrast, this paper provides a detailed examination of structural features that illuminate important physical processes that arise in the course of the highly unsteady separation process from the curved hill surface.

Conventionally, the structural features of flow fields predicted with simulation techniques is visualised (or attempted

to be visualised) by means of (combinations of) iso-contours for vorticity, pressure and/or several structure-identification criteria, such as " $Q$ " or " $\lambda_2$ "<sup>1</sup>. At low Reynolds numbers, these methods are quite effective, as the flow is dominated by relatively large-scale structures embedded within a rather smooth "background flow". However, at high values of the Reynolds number, the flow tends to be very complex and fine-grained, containing structures that span a broad range of length and time scales. In such circumstances, conventional visualisation methods are much less effective or, indeed, entirely ineffective. Here, we illustrate the effectiveness of using a low-order representation of the predicted flow using Proper Orthogonal Decomposition (POD). This method is usually used to reduce the amount of information required to describe complex turbulent flows, by focusing on the most energetic scales. Here, the focus is on applying this method to highlight major structural features. Another novel feature of the present work is that the Reynolds-number dependence of the structures is investigated, over a range spanning from low to moderately high values, for a fixed geometric configurations, based on data derived from a set of simulations. This is in contrast to studies of Acarlar and Smith (1987) who focused on low Reynolds numbers only and Persson et al (2006) who have studied the same test case as that considered herein, but at a single Reynolds number. For turbulent boundary layers on flat plate, Liu et al. (1994) have shown experimentally that the one-dimensional spectra of the POD in the outer part of a boundary layer are independent of the Reynolds number. This indicates that the "heads" of the hairpin vortices, which protrude into the outer reaches of the log-law region, evolve independently of the inner layer. Whether this insensitivity to Reynolds number applies here too is one issue that is addressed below, using flow visualisation following filtering out of small scale (low-energy) features of the flow via POD.

## FLOW CONFIGURATION AND NUMERICAL METHODS

Fig. 1 shows the geometry of the three-dimensional hill, the 1.5-million-node mesh used to discretize the flow domain and major mean-flow characteristics in the separated region on the leeward side of the hill. The circular hill has a height-to-base ration of 4, and is located in a duct of size ( $16H \times 3.205H \times 11.67H$ ), with  $H$  being the hill height. At the intermediate and highest Reynolds number, the wall-normal distance of the mesh plane closest to the wall is located at around  $y^+ = 5$  and 50, respectively. In both cases, and especially the higher Reynolds-number value, this necessitated the use of a hybrid LES-RANS approach, presented in details in Tessicini et al. (2007).

The flow field was computed using an in-house multi-block, finite volume code within which advection and diffusion are approximated with a second-order central-differencing schemes. Time marching is based on a fractional-step method, with the time derivative being discretized by a second-order backward-biased approximation. The flux terms are advanced explicitly using a second-order Adams-Bashforth method. The velocity field is then corrected via the pressure gradient by a projection onto a divergence-free velocity field. The pressure is computed as a solution to the pressure-Poisson problem by means of a three-dimensional V-cycle multigrid algorithm, operating in conjunction with a successive-line over-relaxation scheme.

<sup>1</sup>We note in passing, however, that is no consensus on what constitute coherent structures (Dubief and Delcayre, 2000)

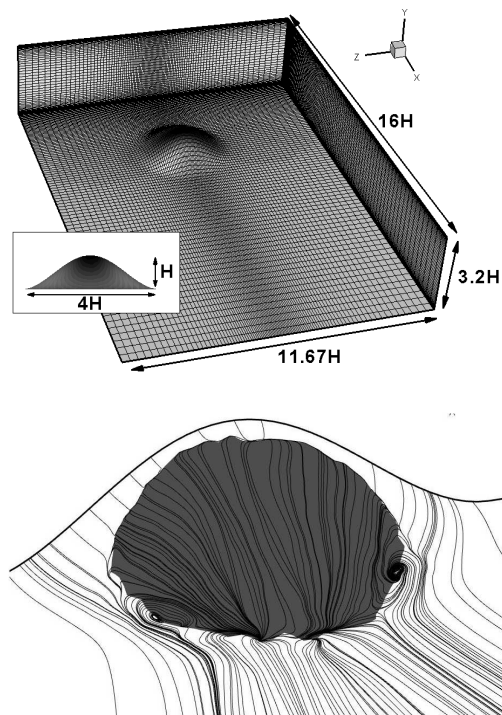


Figure 1: 3D hill geometry, computational domain and mean-flow characteristics (gray region: zero-streamwise-velocity surface).

The code is fully parallelised using MPI and was run on several multi-processor computers, with up to 256 processors.

The inflow conditions were generated using a precursor simulation at one particular Reynolds number, and then rescaled to correspond to the appropriate Reynolds number at which the relevant 3d-hill simulation was performed. The boundary layer thickness ( $\delta_{99}$ ) was kept at 50% of the hill height at all Reynolds numbers, corresponding to the experimental conditions at  $Re = 130,000$ . The rationale of doing so is rooted in the wish to examine, in isolation, the dependence of the flow structure to the Reynolds number.

## POD AND EXTENDED POD

POD was originally applied to turbulent flows, as a statistical-analysis tool, by Lumley (1967). POD, also known as Karhunen-Loève Decomposition or Principal-Component Analysis, is a procedure for extracting a particular basis for a modal decomposition of an ensemble of signals. POD is a linear procedure, which is one of its limitations, but unlike linear-stability theory, it does not rely on any assumptions about the linearity or otherwise of the problem being analysed: a POD analysis essentially operates on data originating from either an experiment or simulation, and it provides a rigorous mathematical basis for extracting spatial and temporal structures, based on predetermined and well-founded criteria. The following summarises the method as far as it pertains to the present study.

A set of realizations of the velocity field  $\mathbf{U}(\mathbf{X})$  on a spatio-temporal domain  $S$  forms the subject of the analysis. The POD modes are obtained by searching the vector field  $\Phi(\mathbf{X}, t)$  (with  $\mathbf{X} = (x, y, z)$ ) that is closest to  $\mathbf{U}$ , on average. Every flow realization can then be decomposed into

the series:

$$U_i(\mathbf{X}, t) = \sum_{n=1}^M a^n(t) \Phi_i^n(\mathbf{X}) \quad (1)$$

where  $i$  denotes the  $i$ -th component of  $\mathbf{U}$ ,  $M$  the number of modes considered,  $\Phi_i^n$  are the eigenvectors and  $a^n$  are the time-dependent coefficients of the decomposition.

The usefulness of POD in fluid mechanics is due to the fact that it provides an optimal decomposition of the kinetic energy integrated over the domain  $S$ , with

$$\langle \mathbf{U}, \mathbf{U} \rangle = \sum_n \lambda^n \quad (2)$$

where  $\lambda^n$  are the eigenvalues associated with the eigenvector  $\Phi_i^n$ .

Two different types of POD are commonly used, depending on the type of signal considered. The direct method, originally proposed by Lumley (1967), uses a spatial correlation tensor, defined by  $R_{ij}(\mathbf{X}, \mathbf{X}') = \langle \mathbf{U}(\mathbf{X}, t), \mathbf{U}(\mathbf{X}', t) \rangle$ , for which the size of the problem is equal to  $N \times N_c$ ,  $N$  being the number of nodal points, and  $N_c$  being the number of components of  $\mathbf{U}$ .

The other method, proposed by Sirovich (1987), is to use a temporal correlation tensor, defined by  $R_{ij}(t, t') = \langle \mathbf{U}(\mathbf{X}, t), \mathbf{U}(\mathbf{X}, t') \rangle$ . The size of the problem is here much smaller, being equal to the number of realisations  $M$  of the flow. This method, called snapshot POD, can be used if the number of points is much greater than the number of snapshots. This is the usual practice adopted for post-processing PIV data, while both methods can be used with similar effectiveness to post-process numerical data. In a separate study on free mixing layers, Lardeau et al. (2007) explain and demonstrate the relative advantages and disadvantages of both methods. It is the latter method that is applied herein to the hill flow.

As the Reynolds number of the hill flow is relatively high, most of the interesting features of flow, especially in the post-separated leeward side of the hill, are of the same order, in terms of energy content, as those in the oncoming boundary layer. Hence, when performing the decomposition, it is not readily possible to separate features originating from these two regions. To overcome this type of difficulty, a modified version of POD, called *Extended POD*, was introduced by Maurel et al. (2001), and then generalized by Boree (2003). This method allows the interaction between different energetic parts associated with different domain portions to be identified. More generally, Boree (2003) has shown that the extended POD can also be used to study the correlation of any quantity with the velocity field. The principle is to compute the POD modes on a domain  $S$  (adopting Boree's notation) and then use the coefficients of the decomposition and the associated eigenvalues to define a new family of modes. In specific terms, the extended modes of the new vector  $\mathbf{V}(\mathbf{X}', t)$  on a domain  $\Gamma$  (identical to or different from  $S$ ) are defined as:

$$\Psi^p(\mathbf{X}') = \frac{\langle a^p(t) \mathbf{V}(\mathbf{X}', t) \rangle}{\lambda^p} \quad (3)$$

where  $a^p(t)$  and  $\lambda^p$  are respectively the random coefficients and the eigenvalues associated with the POD on the domain  $S$  for the quantity  $\mathbf{U}$  (Eq. 1). For time-averaged data, the domains  $S$  and  $\Gamma$  are spatial domains and thus,

$$\Psi^p(\mathbf{X}') = \frac{1}{\lambda^p T} \int_0^T a^p(t) \mathbf{V}(\mathbf{X}', t) dt \quad (4)$$

where  $T$  is the integration time. The following decomposition is used to define the parts of  $\mathbf{V}$  in the domain  $\Gamma$  which is correlated with  $\mathbf{U}$  in the domain  $S$ . An important result presented by Boree (2003) is that  $\mathbf{V}_c$  is the only part of  $\mathbf{V}$  correlated with  $\mathbf{U}$ . The correlated and decorrelated part are given respectively by

$$\begin{aligned} \mathbf{V}_c(\mathbf{X}', t) &= \sum_{n=1}^M a^n \Psi^n(\mathbf{X}') \\ \mathbf{V}_d(\mathbf{X}', t) &= \mathbf{V}(\mathbf{X}', t) - \mathbf{V}_c(\mathbf{X}', t) \end{aligned} \quad (5)$$

This makes the extended POD useful for studying spatial and temporal interactions between different regions and related structures within a single flow.

## RESULTS

Simulations and associated POD processing have been performed for three Reynolds numbers:  $Re=1,300$ ,  $13,000$  and  $130,000$ , based on the hill height and free-stream velocity. In the following, for each Reynolds number, 780 snapshots, extending over a period of 180 time units, have been used to compute the eigenvectors in Eq. (1). While POD spectra have been constructed with up to 780 modes, to examine the distribution of energy across the modes, only the first four modes (excluding the mean flow) have been processed to generate the results to follow, in order to bring out the large-scale structures of the flows. The conditions at the lowest value are transitional, and the simulation is, effectively, a DNS. At the two higher values, the dynamic Smagorinsky model has been used in conjunction with the zonal LES-RANS scheme, the latter allowing a substantial reduction in the computational cost relative to wall-resolved LES. For the highest value, Tessicini et al. (2006) provide a broad range of comparisons with experimental data to demonstrate the predictive effectiveness of the zonal LES-RANS scheme, relative to coarse-mesh and nearly-wall-resolving fine-mesh LES. As observed in Tessicini et al. (2007), the flow at  $Re = 130,000$ , aft of the hill, is characterised by distinctly periodic features which are broadly symmetrical. In the mean, the hill-topology maps contain two distinctive focal points, which indicate that vorticity is shed from the hill surface, with the vortex lines anchored to the hill surface. Both these observations, taken together, suggest the periodic formation, shedding and subsequent stretching of  $\Omega$ -shaped vortical structures of the kind referred to here as "hairpin vortices". The desire to gain better insight into this process has motivated the present POD study and the exploration of its dependence on the Reynolds number.

Fig. 1, lower plot, conveys the principal mean-flow features by way of streaklines and the zero-streamwise-velocity surface for the highest Reynolds number only. For the lowest value (not shown here), the recirculation zone extends well beyond the hill base, up to  $x = 4H$ , with the hill-base radius being at  $x = 2H$ . The topology observed in Fig. 1 is very similar to the one found by Acarlar and Smith (1987) behind a hemisphere. For the two higher values of Reynolds number, the length of the recirculation zone is substantially reduced, due to the fully turbulent state of the flow upstream of the hill crest, with reattachment occurring close to the foot of the hill, at  $\approx 2H$ . However, for all three cases, the streakline patterns are similar, indicating the same qualitative mean-flow features.

The instantaneous flow structure behind the hill is very complex, even at the lowest Reynolds number. Observations

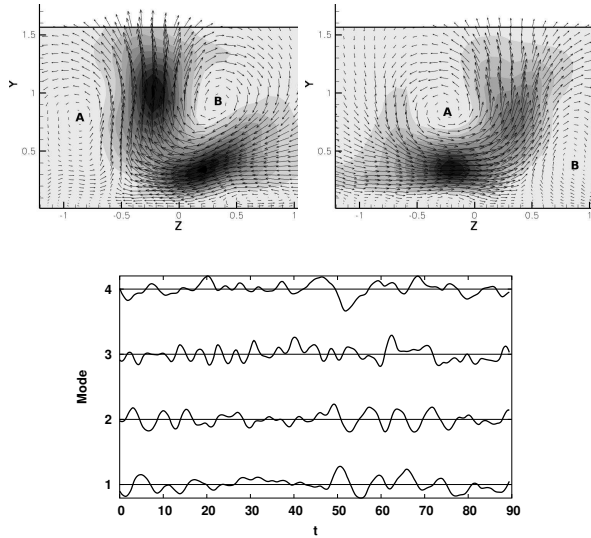


Figure 2:  $Re = 1,300$ ; top: velocity vectors and iso-contours of the kinetic energy in plane  $(y, z)$  located at  $x = 6.15H$ , for the first two modes  $\Phi^1$  and  $\Phi^2$ , Eq. 1, representing 12.5% and 10% of the total energy, respectively; bottom: time-evolution of the coefficients  $a^n(t)$ .

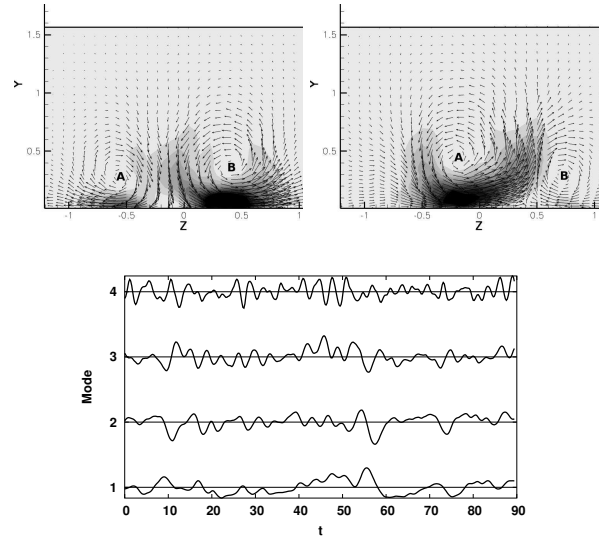


Figure 4:  $Re = 130,000$ ; top: vectors and iso-contours of the kinetic energy in plane  $(y, z)$  located at  $x = 2.75H$ , for the first two modes  $\Phi^1$  and  $\Phi^2$ , Eq. 1, representing 8.5% and 8% of the total energy, respectively; bottom: time-evolution of the coefficients  $a^n(t)$ .

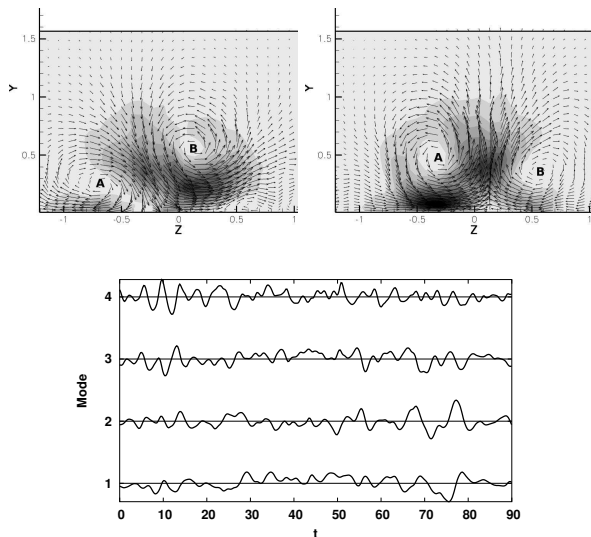


Figure 3:  $Re = 13,000$ ; top: vectors and iso-contours of the kinetic energy in plane  $(y, z)$  located at  $x = 2.75H$ , for the first two modes  $\Phi^1$  and  $\Phi^2$ , Eq. 1, representing 8% and 7% of the total energy, respectively; bottom: time-evolution of the coefficients  $a^n(t)$ .

of laminar flow around hemispheres reveal the formation of a regular train of hairpin vortices, while in the present case, successive vortices shed from the surface around the hill crest interact non-linearly with one another and with small hairpin vortices emanating from the base of the hill.

A differentiation of the structures associated with separation from those within the turbulent boundary layer is possible, in principle, using the “snapshot POD” method applied to the whole 3D-flow domain. At low Reynolds numbers, the energy tends to be concentrated in a few low-order modes, with 30% of the fluctuating energy in the first 6 modes. At higher Reynolds numbers, the number of modes that need to be included to capture the same amount of energy may exceed 20 or 50. These energy levels have been determined from POD energy spectra, which reveal charac-

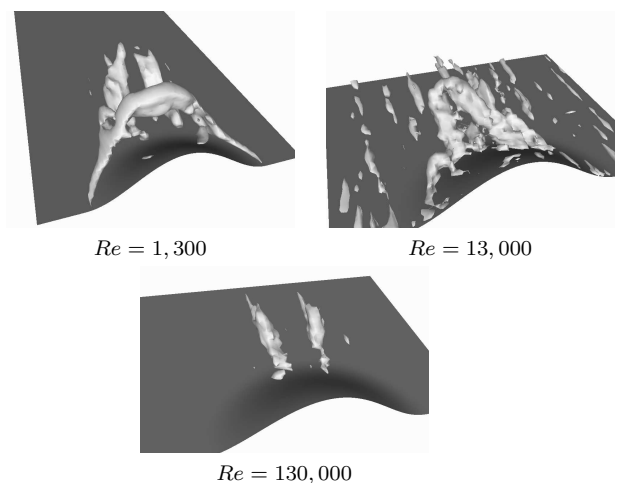


Figure 5: Isosurface of  $Q$ -criterion using the reconstructed field from the first four extended POD modes

teristic  $-11/9$  slopes, consistent with the behaviour observed by Knight and Sirovich (1990) for high Reynolds number and for a wide range of flow configurations. In the present flow, a qualitatively similar slope is found even for the lowest value examined, for which the flow condition is not fully turbulent. The above relationship between modes and levels of energy has unfortunately frustrated efforts to distinguish contributions from separation-related and boundary-layer-inherent structures, the former being relatively weak. Thus, a reconstruction with low-order modes only reveals a combination of large-scale features associated both with separation and with the turbulent boundary layer. An approach found to be more effective than 3D POD is to focus on 2D spanwise planes and then to reconstruct the 3D flow from a succession of 2D POD analyses.

One observation made by Tessicini et al. (2007) was that, at given  $x$  location, two broadly symmetric vortices appeared to be “shed” at regular intervals. Thus, attention is initially focused here on one plane located downstream of the re-

circulation region. Figs. 2, 3 and 4 show the vector field associated with the first two spatial POD modes  $\Phi^1$  and  $\Phi^2$ , as well as the time-evolution traces of the coefficients  $a^n(t)$  associated with the modes  $n=1-4$ . The combination of these two POD elements, in accordance with Eq. (1), gives an approximation of the fluctuating flow field that contains the most energetic structures. Strong similarities are observed among corresponding plots for the three Reynolds numbers. First, modes 1 and 2 both feature two large, (size-wise) asymmetric vortices (denoted  $A$  and  $B$ ). For mode 1, for all Reynolds number, the maximum of energy is located below vortex  $B$  and between the two counter-rotating vortices. As the Reynolds number increases, the centres of the vortices move towards the wall. Mode 2 follows a similar pattern, with the maximum of energy located below vortex  $A$ . More generally, for both modes, the maximum of energy is always located under the largest vortex. Further significant similarities are found in the time traces of the coefficients  $a^n(t)$ . For  $Re = 1,300$ , low-amplitude high-frequencies oscillations are observed between  $t = 30$  and  $t = 48$ , followed by higher amplitude lower-frequency oscillations in the range  $48 < t < 80$ . This is in contrast to  $a^3(t)$  and  $a^4(t)$ , which do not feature a bi-modal character and are dominated by higher frequencies than those in  $a^1(t)$  and  $a^2(t)$ . Similar features also arise for the two other Reynolds numbers. Another interesting observation from the time traces is the time-shift between consecutive modes, especially between modes 1 and 2. This shift is most clearly recognised from Fig. 4 in the time period between  $t = 50 - 90$ . This shift corresponds to a phase angle between modes  $a^1(t)$  and  $a^2(t)$ , and can be interpreted as signifying a tilting of vortices  $A$  and  $B$  from left to right and vice versa, qualitatively similar to the phase angle observed in POD analysis of any von Kàrmàn vortex street.

The level of energy carried by the first four modes in the POD applied to the 2D planes is higher than in the full 3D snapshot POD, and fewer modes are needed to reconstruct a reduced representation that contains a significant proportion of the fluctuating energy. In the following, only the first four modes have been used, representing, collectively, 33%, 24% and 20% of the total energy for the three Reynolds number, respectively. The choice of using this limited number of modes may be justified on the basis of the observed dominance of a few large and regular features in the modes  $\Phi^i$ . For  $i=1$  and 2, only two big vortices are present (Fig. 2, 3 and 4), and for  $i=3$  and 4, four vortices can be observed for all cases (not shown here). For  $i=5$  and above, the number of vortices increases, and these are randomly scattered in the  $(y, z)$  plane, making the reconstruction more “noisy” and less distinct. While this choice of modes is somewhat arbitrary, it is recalled that the aim of this paper is to extract the large-scale features of the flow, rather than to extract features to a particular level of energy.

Iso-surfaces of the  $Q$  criterion at one particular instant in time are shown on Fig. 5. Broadly symmetric hairpin-shaped vortices are clearly seen for the two lower Reynolds numbers, while for the highest value, only two separated legs can be observed. At  $Re = 13,000$ , secondary vortices are present on both sides of the hill. At the highest Reynolds number, the legs do not seem to be attached, and this is confirmed by space-time plots, which indicate that the separation from the top of the hill is dissociated from the legs observed in Fig. 5.

One important drawback of focusing attention on iso-surfaces of one particular quantity at one particular instant is that these only provide a narrow window to the flow

field. In fact, for the highest Reynolds number case (Fig. 5), this visualisation does not represent well the highly dynamic state of the flow. To give a better view, the first four modes were used to reconstruct the flow field at one particular streamwise location and in time, and the result is shown in Fig. 6 in the form of space-time plots of the  $Q$  criterion (the time axis is directed from the back towards the front). For the lowest Reynolds number, hairpin-type structures are clearly shed at a regular frequency, and the shape of consecutive structures is very similar to that seen in Fig. 5, although their orientation is inverted, due to the particular time axis used. POD is very informative and rewarding, for this particular case, as a means of educing the biggest coherent structures of the flow. In fact, all other types of decomposition attempted - e.g. using POD modes built at different streamwise locations or across the  $z$ -wise symmetry plane of the hill - gave similar results. The only significant difference was in the amount of energy represented by the first four modes.

As is evident from Fig. 6, the hairpin-type structures at the two higher Reynolds numbers do not emerge as clearly as they do at the lowest value, especially not at  $Re = 130,000$ . At this value, the vortices corresponding to  $A$  and  $B$  (Fig. 4), shed from the sides of the hill, seem to be completely dissociated from the one shed from the top of the hill, i.e. the one that would normally form the head of the hairpin structure. In fact, this dissociation also applies, to a lesser degree, to the lower Reynolds numbers, and this is why, even if the threshold for the  $Q$ -criterion is progressively reduced, the two legs never fully join in the visualisations of Fig. 6.

One possible explanation for the different behaviour of the reconstructed fields, despite strong similarities in the modes  $\Phi^1$  and  $\Phi^2$ , may be derived from the differences observed in the time-evolution of the modes  $a^1$  and  $a^2$ . For the lowest Reynolds number, Fig. 2 shows that a maximum in the amplitude of mode 1 is always preceded, with a very short time delay, by a maximum for  $a^2$ , and this observation also extends to the minima. Thus, vortices  $A$  and  $B$  are shed at almost the same time. This close to in-phase process also occurs for the intermediate Reynolds number - for example, between  $t = 20$  and  $t = 40$  - and within this period, hairpin-like vortices are observed in Fig. 6. However, when a maximum, positive, value of  $a^1$  corresponds to a minimum, negative, value of  $a^2$  - as occurs at around  $t = 68$  for  $Re = 13,000$  - the spatial modes  $\Phi^1$  and  $\Phi^2$  are not additive but subtractive. This phase inversion is also observed at different positions on Fig. 4 for the highest Reynolds number (at  $t = 10, 22, 85$ , etc.), and this may at least be a contributory reason for the absence of clear symmetric hairpin-shaped structures, as those observed at the lower Reynolds numbers. This phase shifting also indicates that the dynamics at higher Reynolds number are much more complex, even if the low-order POD modes show fundamentally similar features.

## CONCLUSIONS

The structure of a separated flow behind a 3D hill has been investigated by way of 3D and 2D POD analyses, with attention focusing on low-order modes. The main objective has been to illuminate the nature of coherent structures associated with weak periodic events observed in earlier LES computations, and to investigate whether the mechanism is Reynolds-number dependent. A full low-order 3D POD analysis was found to be ineffective in efforts to separate the weak differences between similarly energetic structures origi-

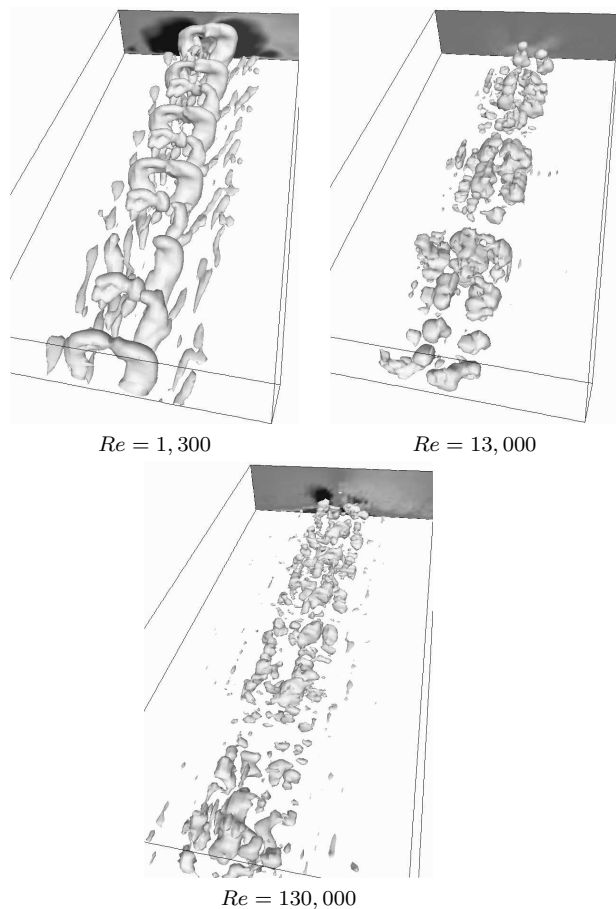


Figure 6: Space-time iso-surfaces of the  $Q$ -criterion using the first four extended-POD modes at  $x = 6.15H$  for  $Re = 1,300$  and at  $x = 2.75H$  for  $Re = 13,000$  and  $130,000$ .

nating from the upstream boundary layer and the separation region. In contrast, 2D POD, applied to selected stream-wise planes, has been shown to offer valuable insight into the evolution of large-scale unsteady structures. Significant similarities in the shape of the POD modes (eigenvectors) have been observed across a wide Reynolds-number range. At moderate Reynolds numbers, the POD analysis has revealed the periodic formation and ejection of large hairpin-like vortices. At the highest Reynolds number, these structures are much less pronounced, but time-traces of the POD coefficients nevertheless show clear evidence of periodic ejections of the same type. The presence (or absence) of clearly defined hairpin-like vortices for the different Reynolds numbers is argued to be linked to particular features in the time evolution of the modes. Further analysis in this direction would be necessary to confirm the nature of the mechanism. Very highly-resolved LES, currently in progress, are expected to offer a better understanding of the flow dynamic for the highest Reynolds number.

#### ACKNOWLEDGEMENTS

The authors are grateful to Drs. N. Li and G. Fishpool for help in the computations and for fruitful discussions on hairpin vortices. The study was partially supported by the DESider project, funded by the CEC Research Directorate General under Contract AST3-CT-2003-502842.

#### REFERENCES

- Acarlar, M.S. and Smith, C.R. A study of hairpin vortices in a laminar boundary layer. part 1. hairpin vortices generated by a hemisphere protuberance. *J. Fluid Mech.*, **175**:1–41, 1987.
- Boree, J. Extended proper orthogonal decomposition: a tool to analyse correlated events in turbulent flows. *Expts. Fluids*, **35**:188–192, 2003.
- Dong, S. and Meng, H. Flow past a trapezoidal tab. *J. Fluid Mech.*, **510**:219–242, 2004.
- Dubief, Y. and Delcayre, F. On coherent-vortex identification in turbulence. *J. of Turb.*, **1**, 2000.
- Hsieh, T. and Wang, K.C. Three-dimensional separated flow structure over a cylinder with a hemispherical cap. *J. Fluid Mech.*, **324**:83–108, 1996.
- Jimenez, J. and Pinelli, A. The autonomous cycle of near-wall turbulence. *J. Fluid Mech.*, **389**:335–359, 1999.
- Knight, B. and Sirovich, L. Kolmogorov inertial range for homogeneous turbulent flows. *Phys. Rev. L.*, **65**(11):1356–1359, 1990.
- Laureau, S., Laizet, S. and Lamballais, E. Effects of velocity ratio on the spatial development of turbulent boundary layers. *J. Fluid Mech.*, in preparation, 2007.
- Liu, S., Meneveau, C. and Katz, J. On the properties of similarity subgrid scale models as deduced from measurements in a turbulent jet. *J. Fluid Mech.*, **275**:83–119, 1994.
- Lumley, J.L. *The structure of inhomogeneous turbulence*. A.M. Yaglom and V.I. Tatarski, Nauka, Moscow, 1967.
- Maurel, S., Boree, J. and Lumley, J.L. Extended proper orthogonal decomposition: application to jet/vortex interaction. *Flow, Turbulence and Combustion*, **67**:125–136, 2001.
- Persson, T., Liefvendahl, M., Bensow, R.E. and Fureby, C. Numerical investigation of the flow over an axisymmetric hill using LES, DES and RANS. *J. of Turb.*, **7**:4, 2006.
- Simpson, R.L., Long, C.H. and Buyn, G. Study of vortical separation from an axisymmetric hill. *Int. J. Heat and Fluid Flow*, **23**(5):582–591, 2002.
- Sirovich, L. Turbulence and the dynamics of coherent structures. part 1: coherent structures. *Quat. J. Appl. Math.*, **45**:561–571, 1987.
- Tessicini, F., Temmerman, L. and Leschziner, M.A. Approximate near-wall treatments based on zonal and hybrid RANS-LES methods for LES at high-Reynolds numbers. *Int. J. Heat and Fluid Flow*, **27**(5):789–799, 2006.
- Tessicini, F., Li, N. and Leschziner, M.A. Large-eddy simulation of three-dimensional flow around a hill-shaped obstruction with a zonal near-wall approximation. *Int. J. Heat and Fluid Flow*, in press, 2007.
- Zhou, J., Adrian, R.J., Balachandar, S. and Kendall, T.M. Mechanisms for generating coherent packets of hairpin vortices in channel flow. *J. Fluid Mech.*, **387**:353–396, 1999.